A Gurson-type layer model for ductile porous solids with isotropic and kinematic hardening

Léo Morin[a,b,*], Jean-Claude Michel[a], Jean-Baptiste Leblond[c]

[a] Laboratoire de Mécanique et d'Acoustique, CNRS, UPR 7051, Aix-Marseille Univ, Centrale Marseille, 4 impasse Nikola Tesla, CS 40006, 13453 Marseille Cedex 13, France
[b] PIMM, Arts et Métiers-ParisTech, CNAM, CNRS, UMR 8006, 151 bd de l'Hôpital, 75013 Paris, France
[c] Sorbonne Universités, Université Pierre et Marie Curie (UPMC), CNRS, UMR 7190, Institut Jean Le Rond d'Alembert, F-75005 Paris, France

Keywords:
Porous ductile solids
Isotropic hardening
Kinematic hardening
Sequential limit-analysis

A B S T R A C T

The aim of this work is to propose a Gurson-type model for ductile porous solids exhibiting isotropic and kinematic hardening. The derivation is based on a "sequential limit-analysis" of a hollow sphere made of a rigid-hardenable material. The heterogeneity of hardening is accounted for by discretizing the cell into a finite number of spherical layers in each of which the quantities characterizing hardening are considered as homogeneous. A simplified version of the model is also proposed, which permits to extend the previous works of Leblond et al. (1995) and Lacroix et al. (2016) for isotropic hardening to mixed isotropic/kinematic hardening. The model is finally assessed through comparison of its predictions with the results of some micromechanical finite element simulations of the same cell. First, the numerical and theoretical overall yield loci are compared for given distributions of isotropic and kinematic pre-hardening. Then the predictions of the model are investigated in evolution problems in which both isotropic and kinematic hardening parameters vary in time. A very good agreement between model predictions and numerical results is found in both cases.

1. Introduction

The failure of metals, whose impact on the integrity of engineering structures need not be stressed, is one of the most challenging problems faced by the scientific and industrial communities. Indeed its analysis and modelling are complex tasks because it is a multiscale problem. Various mechanisms, at the microscale (e.g. structures of dislocations or grain boundaries) and mesoscale (e.g. hard precipitates or voids), can induce damage leading ultimately to macroscopic cracks. In particular, a difficult but essential task consists in providing predictive micromechanically-based models that permit to account for both monotonic and cyclic loadings.

In the case of *ductile* materials considered in this paper, failure essentially takes place in three steps (see e.g. Benzerga and Leblond, 2010; Pineau et al., 2016; Benzerga et al., 2016 for recent reviews of the topic): (i) the nucleation of voids, (ii) their growth, change of shape and rotation, and finally (iii) their coalescence leading to final failure. The modelling of these mechanisms started with the pioneering work of Gurson (1977), who combined homogenization and limit-analysis of a hollow sphere made of a rigid-ideal-plastic isotropic material to derive a model of ductile materials incorporating void growth. This model has been extended in various directions to account for phenomena not included in its original version, notably void shape effects (Gologanu et al., 1993; 1994; 1997; Garajeu et al., 2000; Madou and Leblond, 2012a; 2012b; 2013; Madou et al., 2013), plastic anisotropy (Benzerga and Besson, 2001; Monchiet et al., 2008; Keralavarma and Benzerga, 2010; Morin et al., 2015c) and void coalescence (Thomason, 1985; Tekoglu et al., 2012; Benzerga and Leblond, 2014; Morin et al., 2015b). It has met, in both its original and improved forms, considerable success in the reproduction of experimental tests of failure of ductile materials under *monotonic* loading conditions.

The failure of ductile metals under *cyclic* loadings is less well understood and mastered. Experiments (Schmidt et al., 1991; Kobayashi et al., 1992) have shown that the strain to fracture is considerably lower, for a given load, if it is reached under cyclic conditions rather than monotonically. This reduction of ductility is commonly attributed to an effect of gradual increase of the mean porosity (volume fraction of voids) during each cycle termed the *ratcheting of the porosity*. This phenomenon was first evidenced in micromechanical finite element simulations performed by Gilles et al. (1992) under conditions of constant over-

* Corresponding author.
E-mail address: leo.morin@ensam.eu (L. Morin).

all triaxiality (in absolute value), and later confirmed by several authors (Devaux et al., 1997; Besson and Guillemer-Neel, 2003; Brocks and Steglich, 2003; Rabold and Kuna, 2005; Steglich et al., 2005; Mbiakop et al., 2015; Lacroix et al., 2016). As explained by Lacroix et al. (2016), the ratcheting of the porosity is fundamentally tied to two features of the material behaviour, namely *strain hardening* and *elasticity*. The effect of elasticity, although important in the context of the ratcheting of the porosity under cyclic loadings, will not be considered in this paper, its study and modelling being postponed to a future paper. We shall thus focus exclusively on the effect of strain hardening, as a first step toward a complete modelling of ductile rupture under cyclic loading conditions.

Devaux et al. (1997), among other things, showed that Gurson (1977)'s classical model does not predict the effect of ratcheting of the porosity under cyclic loadings, but a stabilization of the evolution of the porosity right from the first semi-cycle. The explanation of this shortcoming of Gurson (1977)'s model lies in the crude modelling of strain hardening within this model, and more specifically in the fact that the same "average yield stress of the matrix" appears in both the "square" and the "cosh" terms of the yield function. A few theoretical works have tried to improve the modelling of strain hardening effects within Gurson (1977)'s model:

- For *isotropic hardening*, Leblond et al. (1995) proposed a heuristic extension of Gurson (1977)'s yield function involving distinct "average yield stresses of the matrix" in the "square" and "cosh" terms. Their approach was based on some approximate analytical solution to the problem of a hollow sphere made of some rigid-hardenable material and subjected to some arbitrary loading. Their model, which accounts for the heterogeneity of isotropic hardening within the matrix, has notably permitted to qualitatively reproduce the ratcheting of the porosity observed in micromechanical finite element simulations of porous cells subjected to cyclic loadings under conditions of constant overall triaxiality (in absolute value) (Leblond et al., 1995). From a quantitative point of view, however, the comparison was not fully satisfactory. This obviously arose from the fact that the model was not *a priori* designed for cyclic loadings, since it was based on an assumption of *positively* proportional straining which is inadequate for such loadings. This hypothesis was relaxed by Lacroix et al. (2016), at the expense of introduction of radial discretization of an underlying mesoscopic hollow sphere and calculation and storage of the hardening parameters in each of the spherical layers thus defined. This resulted in a much improved agreement of model predictions and results of micromechanical finite element simulations.
- For *kinematic hardening*, Mear and Hutchinson (1985) introduced a macroscopic backstress in Gurson (1977)'s model. However, this backstress was not linked to some heterogeneously distributed microscopic counterpart in the matrix, and its evolution equation was complex: it was adjusted in such a way that the isotropic (Gurson) and kinematic models yielded identical predictions for proportional loadings. The aim of this kinematic model was not to deal with cyclic loadings but rather to evidence the impact of the local curvature of the yield locus upon macroscopic strain localization. This aspect was examined in detail by Becker and Needleman (1986).

The importance of the effect of strain hardening upon ductile failure - and especially the ratcheting of the porosity under cyclic loadings - acts as a strong incentive to develop models accounting better for the heterogeneous distribution of hardening in the plastic matrix. In particular, the incorporation of kinematic hardening appears to be necessary in order to deal with cyclic plasticity (Chaboche, 1991). The development of a Gurson-type, micromechanically-based model accounting for both isotropic and kinematic hardening, with possibly complex evolution laws for the parameters governing the latter type of hardening, seems of great interest to reproduce the failure of ductile metals under cyclic loadings.

The aim of this paper is to derive such a model. It is organized as follows:

- Section 2 presents the basic ingredients of the theoretical approach and notably the "sequential limit-analysis" approach, which extends the methods and results of classical limit-analysis to materials exhibiting strain hardening.
- Section 3 is devoted to the derivation of a Gurson-like "layer model" extending that developed by Lacroix et al. (2016), accounting for both isotropic and kinematic hardening.
- Section 4 finally compares the predictions of the theoretical model to the results of some new micromechanical finite element simulations.

2. Position of the problem

In the major part of the paper, no hypothesis is made whatsoever on the magnitude of the displacements and strains, and a large displacement - large strain formulation is used; $\mathbf{d}$ represents the local Eulerian strain rate and $\boldsymbol{\sigma}$ the local Cauchy stress tensor.

2.1. Geometry, material, admissibility conditions of velocity fields

In order to derive the overall constitutive law of the porous medium, we consider, following Gurson (1977), a spherical "elementary cell" Ω containing a concentric spherical void ω. The porosity (void volume fraction) is defined by

$$f = \frac{\mathrm{vol}(\omega)}{\mathrm{vol}(\Omega)} = \frac{a^3}{b^3}, \tag{1}$$

where a is the void's radius and b the cell's external radius. The spherical coordinates and associated local orthonormal basis are denoted r, θ, φ and $(\mathbf{e}_r, \mathbf{e}_\theta, \mathbf{e}_\varphi)$.

The material is assumed to be rigid-plastic (no elasticity) and exhibit a mixed, isotropic and kinematic hardening; it is thus supposed to obey the following criterion:

$$\phi(\boldsymbol{\sigma}(\mathbf{x})) = (\boldsymbol{\sigma}(\mathbf{x}) - \boldsymbol{\alpha}(\mathbf{x}))^2_{\mathrm{eq}} - \bar{\sigma}^2(\mathbf{x}) \leq 0, \qquad \forall \mathbf{x} \in \Omega - \omega, \tag{2}$$

where $\bar{\sigma}$ is the current yield stress and $(\boldsymbol{\sigma} - \boldsymbol{\alpha})^2_{\mathrm{eq}}$ is defined by

$$(\boldsymbol{\sigma} - \boldsymbol{\alpha})^2_{\mathrm{eq}} = \frac{3}{2}(\boldsymbol{\sigma}' - \boldsymbol{\alpha}) : (\boldsymbol{\sigma}' - \boldsymbol{\alpha}). \tag{3}$$

In this expression, $\boldsymbol{\sigma}' = \boldsymbol{\sigma} - \frac{1}{3}(\mathrm{tr}\,\boldsymbol{\sigma})\mathbf{I}$ (where $\mathbf{I}$ is the second-order unit tensor) is the deviator of $\boldsymbol{\sigma}$, and $\boldsymbol{\alpha}$ is a traceless backstress tensor due to kinematic hardening. The Prandtl–Reuss flow rule associated to the criterion via the normality property reads

$$\mathbf{d} = \dot{\lambda}\frac{\partial \phi}{\partial \boldsymbol{\sigma}}(\boldsymbol{\sigma}) = 3\dot{\lambda}(\boldsymbol{\sigma}' - \boldsymbol{\alpha}), \tag{4}$$

where $\dot{\lambda} \geq 0$ is the plastic multiplier. The evolution equations of the yield stress $\bar{\sigma}$ and the backstress $\boldsymbol{\alpha}$ characterizing kinematic hardening will be presented in due time.

The spherical cell is subjected to conditions of homogeneous boundary strain rate:

$$\mathbf{v}(\mathbf{x}) = \mathbf{D} \cdot \mathbf{x}, \quad \forall \mathbf{x} \in \partial\Omega, \tag{5}$$

where $\mathbf{v}$ denotes the local velocity, $\mathbf{x}$ the present position-vector and $\mathbf{D}$ some overall strain rate tensor.

The velocity must verify the property of incompressibility imposed by the absence of elasticity and the plastic flow rule:

$$\mathrm{tr}\,\mathbf{d}(\mathbf{x}) = \mathrm{div}\,\mathbf{v}(\mathbf{x}) = 0, \quad \forall \mathbf{x} \in \Omega - \omega. \tag{6}$$

2.2. Principles of limit-analysis

Limit-analysis combined with Hill–Mandel homogenization is a convenient framework to derive constitutive equations for porous ductile solids. It permits to effectively operate the scale transition by evidencing the effects of microstructural features at the macroscopic scale.

Classical limit-analysis is limited to rigid-ideal-plastic materials within a small displacement - small strain (linearized) framework. Under such assumptions the macroscopic yield locus can be determined using the classical upper-bound theorem (see e.g. Benzerga and Leblond, 2010). The macroscopic stress and strain rate tensors $\boldsymbol{\Sigma}$ and $\mathbf{D}$ being defined as the volume averages of their microscopic counterparts $\boldsymbol{\sigma}$ and $\mathbf{d}$, the fundamental inequality enunciated by the theorem,

$$\boldsymbol{\Sigma} : \mathbf{D} \ \leq \Pi(\mathbf{D}), \tag{7}$$

leads to the parametric equation of the yield locus

$$\boldsymbol{\Sigma} = \frac{\partial \Pi}{\partial \mathbf{D}}(\mathbf{D}), \tag{8}$$

where $\mathbf{D}$ is arbitrary and independent of $\boldsymbol{\Sigma}$ in inequality (7), but tied to it through the macroscopic constitutive law in Eq. (8). The macroscopic plastic potential $\Pi(\mathbf{D})$ in Eqs. (7) and (8) is defined by:

$$\Pi(\mathbf{D}) = \inf_{\mathbf{v}\in\mathcal{K}(\mathbf{D})} (1-f)\langle \pi(\mathbf{d})\rangle_{\Omega-\omega}, \tag{9}$$

where the notation $\langle . \rangle_{\Omega-\omega}$ stands for volume averaging over the sound volume $\Omega - \omega$. In this definition the set $\mathcal{K}(\mathbf{D})$ consists of those velocity fields $\mathbf{v}$ which are kinematically admissible with $\mathbf{D}$ and verify the property of incompressibility, and $\pi(\mathbf{d})$ is the microscopic plastic potential defined for any traceless $\mathbf{d}$ by the formula

$$\pi(\mathbf{d}) = \sup_{\boldsymbol{\sigma}^*\in\mathcal{C}} \boldsymbol{\sigma}^* : \mathbf{d}, \tag{10}$$

where $\mathcal{C}$ is the microscopic convex domain of reversibility.

Sequential limit-analysis (Yang, 1993; Leu, 2007) heuristically extends the methods and results of classical limit-analysis by incorporating the effects of strain hardening and geometric changes. The idea is, still disregarding elasticity, to consider a hardenable material as the sequence of different, successive rigid-ideal plastic materials. At a given instant, a hardenable material without elasticity behaves, if the hardening and the geometry are considered as fixed, like a rigid-ideal plastic material with some pre-hardening modifying its yield criterion and flow rule. An instantaneous limit-load can thus be determined using the classical limit-analysis theorems. In order to account for changes of the strain hardening and geometry, the local hardening parameters and present positions are then updated approximately using the trial velocity field used in the limit-analysis, integrated in a small time step.

3. A Gurson-type model accounting for isotropic and kinematic hardening

In this section we will use sequential limit-analysis to derive a Gurson-type model incorporating both isotropic and kinematic hardening. Hardening will be introduced locally in the criterion as a fixed pre-hardening, and the resulting instantaneous loads promoting plastic flow of the cell will be evaluated. The hardening parameters in the matrix will then be considered to evolve *a posteriori* according to the trial velocity field adopted in the limit-analysis.

3.1. Macroscopic plastic potential

In order to derive a Gurson-type model accounting for both isotropic and kinematic hardening, we first need to evaluate the macroscopic plastic potential for an initial arbitrary distribution of the quantities characterizing hardening, that is $\bar{\sigma}(\mathbf{x})$ and $\boldsymbol{\alpha}(\mathbf{x})$.

3.1.1. Velocity fields

To approximately calculate the plastic potential, we consider Gurson (1977)'s trial incompressible velocity field[1]

$$\mathbf{v}(\mathbf{x}) = \frac{b^3}{r^2} D_{\mathrm{m}} \mathbf{e}_r + \mathbf{D}' \cdot \mathbf{x}, \tag{11}$$

where $D_{\mathrm{m}} = \frac{1}{3}\operatorname{tr}\mathbf{D}$ denotes the mean overall strain rate and $\mathbf{D}' = \mathbf{D} - D_{\mathrm{m}}\mathbf{I}$ the deviatoric overall strain rate tensor. The associated microscopic strain rate reads

$$\mathbf{d}(\mathbf{x}) = \mathbf{D}' + \frac{b^3}{r^3} D_{\mathrm{m}} (-2\mathbf{e}_r \otimes \mathbf{e}_r + \mathbf{e}_\theta \otimes \mathbf{e}_\theta + \mathbf{e}_\varphi \otimes \mathbf{e}_\varphi). \tag{12}$$

3.1.2. Expression of the approximate plastic potential

Using equations (2) and (10), the value of the microscopic plastic potential $\pi(\mathbf{d})$ is calculated to be, for any traceless $\mathbf{d}$,

$$\pi(\mathbf{d}) = \bar{\sigma} d_{\mathrm{eq}} + \boldsymbol{\alpha} : \mathbf{d}, \tag{13}$$

where the equivalent strain rate d_{eq} is defined by

$$d_{\mathrm{eq}} = \sqrt{\frac{2}{3}\mathbf{d} : \mathbf{d}}. \tag{14}$$

The approximate macroscopic plastic potential thus reads, adopting the trial velocity field defined by Eq. (11) and the associated strain rate $\mathbf{d}$ given by Eq. (12):

$$\begin{aligned} \Pi(\mathbf{D}) &= \frac{1}{\operatorname{vol}(\Omega)} \int_{\Omega-\omega} \pi(\mathbf{d})\, \mathrm{d}\Omega \\ &= \frac{1}{\operatorname{vol}(\Omega)} \int_{\Omega-\omega} (\bar{\sigma} d_{\mathrm{eq}} + \boldsymbol{\alpha} : \mathbf{d})\, \mathrm{d}\Omega = \Pi^{\mathrm{iso}}(\mathbf{D}) + \Pi^{\mathrm{kine}}(\mathbf{D}), \end{aligned} \tag{15}$$

where the "isotropic" and "kinematic" contributions $\Pi^{\mathrm{iso}}(\mathbf{D})$ and $\Pi^{\mathrm{kine}}(\mathbf{D})$ to $\Pi(\mathbf{D})$ are given by

$$\begin{cases} \Pi^{\mathrm{iso}}(\mathbf{D}) = \dfrac{1}{\operatorname{vol}(\Omega)} \displaystyle\int_{\Omega-\omega} \bar{\sigma} d_{\mathrm{eq}}\, \mathrm{d}\Omega \\ \Pi^{\mathrm{kine}}(\mathbf{D}) = \dfrac{1}{\operatorname{vol}(\Omega)} \displaystyle\int_{\Omega-\omega} \boldsymbol{\alpha} : \mathbf{d}\, \mathrm{d}\Omega. \end{cases} \tag{16}$$

Some further approximations are needed in order to evaluate these integrals analytically. One necessary assumption will be that the local hardening parameters are distributed in a certain, specific way within the matrix. The cell is thus considered to be composed of a finite number N of phases distributed in concentric spheres of radii[2] (see Fig. 1)

$$a = r_1 < \ldots < r_i < \ldots < r_{N+1} = b. \tag{17}$$

The phase contained within the interval $[r_i, r_{i+1}]$ is denoted P_i. The distribution of the quantity $\bar{\sigma}$ characterizing isotropic hardening will be considered as homogeneous in each phase P_i. The distribution of the quantity $\boldsymbol{\alpha}$ characterizing kinematic hardening will also be considered as "homogeneous" in each P_i, in a more elaborate sense specified below.

It should be noted that this kind of approach is basically similar, in the context of ductile rupture, to that of Herve and Zaoui (1993), in the context of Eshelby's inclusion problem.

[1] The component proportional to D_{m} of this velocity field reproduces the exact solution for a hollow sphere made of plastic material (with or without hardening) and subjected to a hydrostatic loading.

[2] The thickness of the phases is not necessarily uniform and may be chosen arbitrarily.

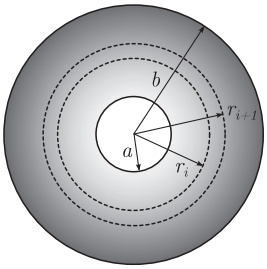

Fig. 1. Hollow sphere: definition of some geometric parameters.

3.1.3. Calculation of the isotropic contribution Π^{iso}

The expression $(16)_1$ of the isotropic part $\Pi^{\mathrm{iso}}(\mathbf{D})$ of the macroscopic plastic potential reads

$$\Pi^{\mathrm{iso}}(\mathbf{D}) = \frac{1}{\mathrm{vol}(\Omega)} \int_a^b 4\pi r^2 \bar{\sigma} \langle d_{\mathrm{eq}}(r) \rangle_{S(r)} \, \mathrm{d}r, \tag{18}$$

where the symbol $\langle . \rangle_{S(r)}$ denotes an average value over the sphere $S(r)$ of radius r.

In order to evaluate analytically the integral in Eq. (18), we use Gurson (1977)'s classical approximation detailed by Benzerga and Leblond (2010) and Leblond and Morin (2014); the potential is evaluated as:

$$\begin{aligned} \Pi^{\mathrm{iso}}(\mathbf{D}) &\simeq \frac{1}{\mathrm{vol}(\Omega)} \int_a^b 4\pi r^2 \bar{\sigma} \sqrt{\langle d_{\mathrm{eq}}^2(r) \rangle_{S(r)}} \, \mathrm{d}r \\ &= \frac{1}{\mathrm{vol}(\Omega)} \int_a^b 4\pi r^2 \bar{\sigma} \sqrt{D_{\mathrm{eq}}^2 + \frac{4b^6}{r^6} D_{\mathrm{m}}^2} \, \mathrm{d}r. \end{aligned} \tag{19}$$

In order to calculate the potential $\Pi^{\mathrm{iso}}(\mathbf{D})$, we introduce the following approximation on the spatial distribution of the yield limit $\bar{\sigma}$:

$\mathcal{A}_1$: *In each phase P_i, the yield limit $\bar{\sigma} = \bar{\sigma}^i$ is considered as uniform.*

The expression (19) of the isotropic part $\Pi^{\mathrm{iso}}(\mathbf{D})$ of the macroscopic plastic potential can thus be simplified into:

$$\Pi^{\mathrm{iso}}(\mathbf{D}) \simeq \sum_{i=1}^{N} \Pi_i^{\mathrm{iso}}(\mathbf{D}), \tag{20}$$

where the "partial" isotropic potential $\Pi_i^{\mathrm{iso}}(\mathbf{D})$ in phase P_i is given by

$$\Pi_i^{\mathrm{iso}}(\mathbf{D}) = \frac{3\bar{\sigma}^i}{b^3} \int_{r_i}^{r_{i+1}} r^2 \sqrt{D_{\mathrm{eq}}^2 + \frac{4b^6}{r^6} D_{\mathrm{m}}^2} \, \mathrm{d}r, \tag{21}$$

or equivalently upon use of the change of variable $u = b^3/r^3$, by

$$\Pi_i^{\mathrm{iso}}(\mathbf{D}) = \bar{\sigma}^i \int_{b^3/r_i^3}^{b^3/r_{i+1}^3} \sqrt{D_{\mathrm{eq}}^2 + 4D_{\mathrm{m}}^2 u^2} \, \frac{\mathrm{d}u}{u^2}. \tag{22}$$

Define now the "local volume fraction" f_i as

$$f_i = \left(\frac{r_i}{b} \right)^3. \tag{23}$$

The expression of the partial isotropic potential then becomes

$$\begin{aligned} \Pi_i^{\mathrm{iso}}(\mathbf{D}) &= \bar{\sigma}^i \int_{1/f_{i+1}}^{1/f_i} \sqrt{D_{\mathrm{eq}}^2 + 4D_{\mathrm{m}}^2 \, u^2} \, \frac{\mathrm{d}u}{u^2} \\ &= \bar{\sigma}^i \left[-\sqrt{\frac{D_{\mathrm{eq}}^2}{u^2} + 4D_{\mathrm{m}}^2} + 2D_{\mathrm{m}} \ln \left(\frac{2D_{\mathrm{m}} u}{D_{\mathrm{eq}}} + \sqrt{1 + \frac{4D_{\mathrm{m}}^2 \, u^2}{D_{\mathrm{eq}}^2}} \right) \right]_{u=1/f_{i+1}}^{u=1/f_i}. \end{aligned} \tag{24}$$

3.1.4. Calculation of the kinematic contribution Π^{kine}

In order to calculate the kinematic part $\Pi^{\mathrm{kine}}(\mathbf{D})$ of the potential, we introduce the following approximation on the spatial distribution of the backstress $\boldsymbol{\alpha}$:

$\mathcal{A}_2$: *In phase P_i, the backstress $\boldsymbol{\alpha}$ is of the form:*

$$\boldsymbol{\alpha} = \boldsymbol{\alpha}^i = \mathbf{A}_1^i + A_2^i (-2\mathbf{e}_r \otimes \mathbf{e}_r + \mathbf{e}_\theta \otimes \mathbf{e}_\theta + \mathbf{e}_\varphi \otimes \mathbf{e}_\varphi), \tag{25}$$

where $\mathbf{A}_1^i$ is a second-order traceless tensor and A_2^i a scalar, both uniform within P_i. (Note that the term $A_2^i(-2\mathbf{e}_r \otimes \mathbf{e}_r + \mathbf{e}_\theta \otimes \mathbf{e}_\theta + \mathbf{e}_\varphi \otimes \mathbf{e}_\varphi)$ is *not* uniform since the vectors $\mathbf{e}_r$, $\mathbf{e}_\theta$, $\mathbf{e}_\varphi$ vary within P_i). It should be noted that the form considered in Eq. (25) has been chosen in order to be compatible with the microscopic strain rate given by Eq. (12). This is a reasonable choice since the rate of the backstress depends on the microscopic strain rate, regardless of the model considered for kinematic hardening.

The expression $(16)_2$ of the kinematic potential $\Pi^{\mathrm{kine}}(\mathbf{D})$ then becomes

$$\begin{aligned} \Pi^{\mathrm{kine}}(\mathbf{D}) &= \frac{1}{\mathrm{vol}(\Omega)} \int_a^b 4\pi r^2 \langle \boldsymbol{\alpha} : \mathbf{d} \rangle_{S(r)} \mathrm{d}r \\ &= \frac{1}{\mathrm{vol}(\Omega)} \sum_{i=1}^{N} \int_{r_i}^{r_{i+1}} 4\pi r^2 \langle \boldsymbol{\alpha}^i : \mathbf{d} \rangle_{S(r)} \mathrm{d}r. \end{aligned} \tag{26}$$

Let us first study the quantity $\langle \boldsymbol{\alpha}^i : \mathbf{d} \rangle_{S(r)}$:

$$\begin{aligned} &\langle \boldsymbol{\alpha}^i : \mathbf{d} \rangle_{S(r)} = \mathbf{A}_1^i : \mathbf{D}' + A_2^i \frac{b^3}{r^3} D_{\mathrm{m}} \langle \mathbf{b} : \mathbf{b} \rangle_{S(r)} \\ &\text{where} \quad \mathbf{b} = -2\mathbf{e}_r \otimes \mathbf{e}_r + \mathbf{e}_\theta \otimes \mathbf{e}_\theta + \mathbf{e}_\varphi \otimes \mathbf{e}_\varphi. \end{aligned} \tag{27}$$

In this expression the property $\langle \mathbf{b} \rangle_{S(r)} = 0$ has been used (Gurson, 1977). One then gets upon calculation of $\langle \mathbf{b} : \mathbf{b} \rangle_{S(r)}$:

$$\langle \boldsymbol{\alpha}^i : \mathbf{d} \rangle_{S(r)} = \mathbf{A}_1^i : \mathbf{D}' + 6A_2^i \frac{b^3}{r^3} D_{\mathrm{m}}. \tag{28}$$

It follows that

$$\begin{aligned} \Pi^{\mathrm{kine}}(\mathbf{D}) &= \sum_{i=1}^{N} \frac{3}{b^3} \int_{r_i}^{r_{i+1}} \mathbf{A}_1^i : \mathbf{D}' \, r^2 \mathrm{d}r \\ &\quad + \sum_{i=1}^{N} \int_{r_i}^{r_{i+1}} 18 A_2^i D_{\mathrm{m}} \frac{\mathrm{d}r}{r} = \mathbf{A}_1 : \mathbf{D}' + 3A_2 D_{\mathrm{m}}, \end{aligned} \tag{29}$$

where

$$\begin{cases} \mathbf{A}_1 = \displaystyle\sum_{i=1}^{N} \mathbf{A}_1^i (f_{i+1} - f_i) \\ A_2 = \displaystyle\sum_{i=1}^{N} 2A_2^i \ln \left(\frac{f_{i+1}}{f_i} \right). \end{cases} \tag{30}$$

3.2. Macroscopic yield criterion

The macroscopic yield criterion is given by the parametric equation

$$\boldsymbol{\Sigma} = \frac{\partial (\Pi^{\mathrm{iso}} + \Pi^{\mathrm{kine}})}{\partial \mathbf{D}} (\mathbf{D}) = \boldsymbol{\Sigma}^{\mathrm{iso}} + \boldsymbol{\Sigma}^{\mathrm{kine}}, \tag{31}$$

where the "isotropic" and "kinematic" contributions $\boldsymbol{\Sigma}^{\mathrm{iso}}$ and $\boldsymbol{\Sigma}^{\mathrm{kine}}$ to the stress $\boldsymbol{\Sigma}$ are defined by

$$\begin{cases} \boldsymbol{\Sigma}^{\mathrm{iso}} = \dfrac{\partial \Pi^{\mathrm{iso}}}{\partial \mathbf{D}} (\mathbf{D}) \\ \boldsymbol{\Sigma}^{\mathrm{kine}} = \dfrac{\partial \Pi^{\mathrm{kine}}}{\partial \mathbf{D}} (\mathbf{D}). \end{cases} \tag{32}$$

Isotropic contribution. Since the isotropic contribution to the plastic potential $\Pi^{\text{iso}}(\mathbf{D})$ depends only on D_{m} and D_{eq}, the isotropic stress $\boldsymbol{\Sigma}^{\text{iso}}$ reads

$$\begin{aligned}\boldsymbol{\Sigma}^{\text{iso}} &= \frac{\partial \Pi^{\text{iso}}}{\partial D_{\text{m}}}\frac{\partial D_{\text{m}}}{\partial \mathbf{D}} + \frac{\partial \Pi^{\text{iso}}}{\partial D_{\text{eq}}}\frac{\partial D_{\text{eq}}}{\partial \mathbf{D}} = \frac{1}{3}\frac{\partial \Pi^{\text{iso}}}{\partial D_{\text{m}}}\mathbf{I} + \frac{\partial \Pi^{\text{iso}}}{\partial D_{\text{eq}}}\frac{2\mathbf{D}'}{3D_{\text{eq}}} \\ &= \Sigma_{\text{m}}^{\text{iso}}\mathbf{I} + \Sigma_{\text{eq}}^{\text{iso}}\frac{2\mathbf{D}'}{3D_{\text{eq}}},\end{aligned} \tag{33}$$

where the mean and equivalent isotropic contributions $\Sigma_{\text{m}}^{\text{iso}}$ and $\Sigma_{\text{eq}}^{\text{iso}}$ to the stress are defined by

$$\begin{cases}\Sigma_{\text{m}}^{\text{iso}} = \dfrac{1}{3}\dfrac{\partial \Pi^{\text{iso}}}{\partial D_{\text{m}}} = \displaystyle\sum_{i=1}^{N}\Sigma_{\text{m},i}^{\text{iso}} \\ \Sigma_{\text{eq}}^{\text{iso}} = \dfrac{\partial \Pi^{\text{iso}}}{\partial D_{\text{eq}}} = \displaystyle\sum_{i=1}^{N}\Sigma_{\text{eq},i}^{\text{iso}}\end{cases} \tag{34}$$

with

$$\begin{cases}\Sigma_{\text{m},i}^{\text{iso}} = \dfrac{1}{3}\dfrac{\partial \Pi_i^{\text{iso}}}{\partial D_{\text{m}}} = \dfrac{2}{3}\bar{\sigma}^i\left[\ln\left(2\xi u + \sqrt{4\xi^2u^2+1}\right)\right]_{u=1/f_{i+1}}^{u=1/f_i} \\ \Sigma_{\text{eq},i}^{\text{iso}} = \dfrac{\partial \Pi_i^{\text{iso}}}{\partial D_{\text{eq}}} = \bar{\sigma}^i\left[-\sqrt{4\xi^2+\dfrac{1}{u^2}}\right]_{u=1/f_{i+1}}^{u=1/f_i}\end{cases}, \xi = \frac{D_{\text{m}}}{D_{\text{eq}}}. \tag{35}$$

Eqs. (34) and (35) provide a parametric representation of the quantities $\Sigma_{\text{m}}^{\text{iso}}$ and $\Sigma_{\text{eq}}^{\text{iso}}$, ξ acting as a parameter.

Kinematic contribution. The calculation of the kinematic stress $\boldsymbol{\Sigma}^{\text{kine}}$ is straightforward and yields

$$\boldsymbol{\Sigma}^{\text{kine}} = \frac{\partial \Pi^{\text{kine}}}{\partial \mathbf{D}} = \mathbf{A}_1 + A_2\mathbf{I}. \tag{36}$$

Summary. By Eqs. (31), (33) and (36), the macroscopic stress inducing plastic flow is given by

$$\boldsymbol{\Sigma} - (\mathbf{A}_1 + A_2\mathbf{I}) = \Sigma_{\text{m}}^{\text{iso}}\mathbf{I} + \Sigma_{\text{eq}}^{\text{iso}}\frac{2\mathbf{D}'}{3D_{\text{eq}}}. \tag{37}$$

Separating the mean and deviatoric parts in this expression and calculating the "von Mises norm" of the latter part, one obtains the macroscopic yield locus in the parametric form

$$\begin{cases}\Sigma_{\text{m}} - A_2 = \Sigma_{\text{m}}^{\text{iso}}(\xi) \\ (\boldsymbol{\Sigma} - \mathbf{A}_1)_{\text{eq}} = \Sigma_{\text{eq}}^{\text{iso}}(\xi),\end{cases} \tag{38}$$

where $\Sigma_{\text{m}}^{\text{iso}}$, $\Sigma_{\text{eq}}^{\text{iso}}$, $\mathbf{A}_1$ and A_2 are given by Eqs. (34), (35) and (30).

3.3. Flow rule

Since the property of normality of the flow rule is preserved in the homogenization procedure (see Gurson, 1977), it reads

$$\mathbf{D} = \dot{\Lambda}\frac{\partial \Phi}{\partial \boldsymbol{\Sigma}}(\boldsymbol{\Sigma}) \quad , \quad \dot{\Lambda}\begin{cases} = & 0 & \text{if} & \Phi(\boldsymbol{\Sigma}) < 0 \\ \geq & 0 & \text{if} & \Phi(\boldsymbol{\Sigma}) = 0,\end{cases} \tag{39}$$

where $\mathbf{D}$ denotes the plastic Eulerian strain rate, $\dot{\Lambda}$ the plastic multiplier and $\Phi(\boldsymbol{\Sigma})$ the macroscopic yield function.

It is worth noting that writing the flow rule (39) explicitly is more difficult than it seems at first sight, since the yield locus is defined by the *parametric* equations (38), the corresponding yield function Φ having no *explicit* expression. Morin et al. (2015a) have analyzed this problem for a parametric criterion of the form (38) and shown that the flow rule may be rewritten, with a suitable re-definition of the plastic multiplier being now denoted $\dot{\tilde{\Lambda}}$, in the following parametric form:

$$\mathbf{D} = \dot{\tilde{\Lambda}}\left(-\frac{1}{3}\frac{\mathrm{d}\Sigma_{\text{eq}}^{\text{iso}}}{\mathrm{d}\xi}(\xi)\mathbf{I} + \frac{\mathrm{d}\Sigma_{\text{m}}^{\text{iso}}}{\mathrm{d}\xi}(\xi)\frac{3}{2}\frac{\boldsymbol{\Sigma}' - \mathbf{A}_1}{\Sigma_{\text{eq}}^{\text{iso}}(\xi)}\right), \tag{40}$$

where $\boldsymbol{\Sigma}'$ is the deviator of $\boldsymbol{\Sigma}$.

3.4. Evolution of hardening parameters

Isotropic hardening. Let g_1 denote the function providing the local yield limit $\bar{\sigma}$ of the matrix as a function of the local cumulated plastic strain p:

$$\bar{\sigma} = g_1(p). \tag{41}$$

We introduce the following approximation on the evolution of isotropic hardening:

$\mathcal{A}_3$: *The "mean yield limit" $\bar{\sigma}^i$ in phase P_i is then supposed to depend on some average value $\bar{p}^i$ of the cumulated plastic strain in this phase, through the formula*

$$\bar{\sigma}^i = g_1(\bar{p}^i). \tag{42}$$

The cumulated plastic strain $\bar{p}^i$ is taken on the mid-surface of the spherical shell occupied by phase P_i, that is at the radial position $\bar{r}_i = \frac{1}{2}(r_i + r_{i+1})$; its expression reads

$$\bar{p}^i = \int_0^t \bar{d}_{\text{eq}}^i(\tau)\mathrm{d}\tau, \tag{43}$$

where $\bar{d}_{\text{eq}}^i$ is the average equivalent plastic strain rate at the position $\bar{r}_i$ associated to Gurson's trial velocity field:

$$\bar{d}_{\text{eq}}^i = \langle d_{\text{eq}}\rangle_{S(\bar{r}_i)} \approx \sqrt{\langle d_{\text{eq}}^2\rangle_{S(\bar{r}_i)}} = \sqrt{D_{\text{eq}}^2 + 4\frac{b^6}{\bar{r}_i^6}D_{\text{m}}^2}, \tag{44}$$

where Gurson's classical approximation has again been used.

In particular, for a power-law isotropic hardening, the function $g_1(p)$ is given by

$$g_1(p) = \bar{\sigma}_0 + hp^m, \tag{45}$$

where $\bar{\sigma}_0$ is the initial yield stress, h the isotropic hardening parameter and m the hardening exponent.

Kinematic hardening. Let $\mathbf{g}_2$ denote the function providing the local rate $\dot{\boldsymbol{\alpha}}$ of the backstress $\boldsymbol{\alpha}$ as a function of this backstress itself, the strain rate $\mathbf{d}$, the cumulated plastic strain p and the equivalent plastic strain rate d_{eq}:

$$\dot{\boldsymbol{\alpha}} = \mathbf{g}_2(\boldsymbol{\alpha}, \mathbf{d}, p, d_{\text{eq}}). \tag{46}$$

Note that the function $\mathbf{g}_2$ must be homogeneous of degree 1 with respect to the strain rate $\mathbf{d}$ since only rate-independent behaviors are considered in the limit-analysis theory.

We introduce the following approximation on the evolution of kinematic hardening:

$\mathcal{A}_4$: *The rate $\dot{\boldsymbol{\alpha}}_i$ of the backstress $\boldsymbol{\alpha}_i$ in phase P_i is then supposed to depend locally on this backstress itself, the plastic strain rate $\mathbf{d}^i$ and some average values $\bar{p}^i$, $\bar{d}_{\text{eq}}^i$ of the cumulated plastic strain and equivalent plastic strain rate in this phase through the formula*

$$\dot{\boldsymbol{\alpha}}_i = \mathbf{g}_2(\boldsymbol{\alpha}^i, \mathbf{d}^i, \bar{p}^i, \bar{d}_{\text{eq}}^i). \tag{47}$$

We again take the strain rate $\mathbf{d}^i$ on the mid-surface of the spherical shell defining phase P_i:

$$\mathbf{d}^i(\theta, \varphi) = \mathbf{d}(\bar{r}_i, \theta, \varphi) \quad \forall(\theta, \varphi), \tag{48}$$

and the average values $\bar{p}^i$, $\bar{d}_{\text{eq}}^i$ of the cumulated plastic strain and equivalent plastic strain rate are defined by Eqs. (43) and (44), respectively.

Eq. (47) is based on the implicit assumption that the form postulated for $\dot{\boldsymbol{\alpha}}_i$ is compatible with that postulated for $\boldsymbol{\alpha}_i$, Eq. (25). This is *not* the case for all possible functions $\mathbf{g}_2$. However the forms (25) and (47) *are* compatible for Armstrong and Frederick (1966)'s quite (though not fully) general kinematic hardening law,

$$\mathbf{g}_2(\boldsymbol{\alpha}, \mathbf{d}, p, d_{\text{eq}}) = c(p)\mathbf{d} - k(p)\boldsymbol{\alpha}d_{\text{eq}}, \tag{49}$$

where $c(p)$ is the "kinematic hardening slope" and $k(p)$ the "strain recovery parameter" (which may both depend on p). For such a

law combination of equations (25) and (47) leads to the following evolution equations for the parameters $\mathbf{A}_1^i$ and A_2^i:

$$\begin{cases} \dot{\mathbf{A}}_1^i = c(\bar{p}^i)\mathbf{D}' - k(\bar{p}^i)\mathbf{A}_1^i \sqrt{D_{\text{eq}}^2 + 4\dfrac{b^6}{\bar{r}_i^6} D_{\text{m}}^2} \\ \dot{A}_2^i = c(\bar{p}^i)\dfrac{b^3}{\bar{r}_i^3} D_{\text{m}} - k(\bar{p}^i) A_2^i \sqrt{D_{\text{eq}}^2 + 4\dfrac{b^6}{\bar{r}_i^6} D_{\text{m}}^2}, \end{cases} \tag{50}$$

where Eqs. (12) and (44) have been used.

3.5. Evolution of geometrical parameters

The evolution of the porosity is classically given by

$$\dot{f} = (1-f)\,\text{tr}\,\mathbf{D}. \tag{51}$$

The proposed approximate evolution equation of the internal radii reads

$$\dot{\bar{r}}_i = \frac{\bar{r}_i}{f_i} D_{\text{m}}. \tag{52}$$

Note that this equation accounts for the geometry changes due to the *sole hydrostatic part* of the loading.

3.6. A simplified version of the model and its link with Leblond et al. (1995)'s model

3.6.1. Leblond et al. (1995)'s model for isotropic hardening

Leblond et al. (1995) proposed to replace Gurson (1977)'s heuristic approach to isotropic hardening effects in porous ductile materials (briefly recalled in Appendix A) with some micromechanical approach based on some approximate analytical solution to the problem of a hollow sphere made of some rigid-hardenable material and subjected to some arbitrary loading. The criterion they obtained was a heuristic extension of that of Gurson (1977) involving distinct "average yield stresses of the matrix" in the "square" and "cosh" terms of the yield function:

$$\frac{\Sigma_{\text{eq}}^2}{\Sigma_1^2} + 2f\cosh\left(\frac{3}{2}\frac{\Sigma_{\text{m}}}{\Sigma_2}\right) - 1 - f^2 = 0, \tag{53}$$

where Σ_1 and Σ_2 are macroscopic internal variables connected to the spatial distribution of the local yield stress $\bar{\sigma}$. These variables govern the yielding in purely deviatoric and purely hydrostatic loadings, respectively:

- For a purely deviatoric loading ($\Sigma_{\text{m}} = 0$), the value $\Sigma_{\text{eq}}^{\text{LPD}}$ of the overall yield stress is given by
$$\Sigma_{\text{eq}}^{\text{LPD}} = (1-f)\Sigma_1. \tag{54}$$
- For a purely hydrostatic loading ($\Sigma_{\text{eq}} = 0$), the value $\Sigma_{\text{m}}^{\text{LPD}}$ of the overall yield stress is given by
$$\Sigma_{\text{m}}^{\text{LPD}} = -\frac{2}{3}\Sigma_2 \ln f. \tag{55}$$

In the original version of the model (Leblond et al., 1995), the expressions of Σ_1 and Σ_2 were obtained in two steps, using the approximate solution of the hollow hardenable sphere problem referred to above. First, Σ_1 and Σ_2 were expressed as functions of the distribution of the local yield stress, using estimates of the overall yield stresses of the hollow sphere under purely deviatoric and purely hydrostatic loadings. Second, the distribution of the local yield stress resulting from the previous mechanical history was obtained in an analytical form under the assumption of positively proportional straining. Although the model did provide a better description of isotropic strain hardening effects in plastic porous materials than that of Gurson recalled in Appendix A, its predictions for cyclic loadings were found to only qualitatively capture the ratcheting of the porosity observed in numerical micromechanical simulations (Devaux et al., 1997), the quantitative agreement remaining mediocre. The explanation was, of course, the inadequacy of the hypothesis of *positively* proportional straining in the case of cyclic loadings.

In an improved version of the model (Lacroix et al., 2016), the hypothesis of positively proportional straining was dropped. In the absence of any specific hypothesis on the evolution of strain in time, the analytical calculation of the distribution of the local yield stress resulting from the previous mechanical history was no longer possible and numerical integration became necessary. The spherical cell was therefore discretized radially - exactly like in the layer model developed here which extends the idea so as to incorporate kinematic hardening. Using our notations, the expressions of Σ_1 and Σ_2 were given by Lacroix et al. (2016) as

$$\begin{cases} \Sigma_1 = \dfrac{1}{1-f}\displaystyle\sum_{i=1}^{N} \bar{\sigma}^i (f_{i+1} - f_i) \\ \Sigma_2 = -\dfrac{1}{\ln f}\displaystyle\sum_{i=1}^{N} \bar{\sigma}^i \ln\left(\dfrac{f_{i+1}}{f_i}\right). \end{cases} \tag{56}$$

3.6.2. A simplified version of the model

It is worth noting that in the case of purely isotropic hardening, the limit-loads given by the parametric criterion (38) coincide exactly with the predictions of Leblond et al. (1995)'s model, for both purely hydrostatic and purely deviatoric loadings. Indeed:

- *Hydrostatic loading.* In this case, the parameter ξ goes to infinity. The limit-load then reads
$$\Sigma_{\text{m}}^{\text{iso}}(\xi \to \infty) = \frac{2}{3}\sum_{i=1}^{N} \bar{\sigma}^i \ln\left(\frac{f_{i+1}}{f_i}\right) = \Sigma_{\text{m}}^{\text{LPD}}. \tag{57}$$
- *Deviatoric loading.* In this case, the parameter ξ is equal to zero. The limit-load then reads
$$\Sigma_{\text{eq}}^{\text{iso}}(\xi = 0) = \sum_{i=1}^{N} \bar{\sigma}^i (f_{i+1} - f_i) = \Sigma_{\text{eq}}^{\text{LPD}}. \tag{58}$$

A natural idea is then to replace the *parametric* form given by Eq. (38) for $\Sigma_{\text{m}}^{\text{iso}}(\xi)$ and $\Sigma_{\text{eq}}^{\text{iso}}(\xi)$ by the simpler *explicit* yield function proposed by Leblond et al. (1995). We thus propose a simplified version of the model involving the explicit criterion

$$\frac{(\Sigma_{\text{eq}}^{\text{iso}})^2}{\Sigma_1^2} + 2f\cosh\left(\frac{3}{2}\frac{\Sigma_{\text{m}}^{\text{iso}}}{\Sigma_2}\right) - 1 - f^2 = 0, \tag{59}$$

or equivalently by equations (38):

$$\frac{(\boldsymbol{\Sigma} - \mathbf{A}_1)_{\text{eq}}^2}{\Sigma_1^2} + 2f\cosh\left(\frac{3}{2}\frac{\Sigma_{\text{m}} - A_2}{\Sigma_2}\right) - 1 - f^2 = 0, \tag{60}$$

where Σ_1, Σ_2, $\mathbf{A}_1$ and A_2 are given by Eqs. (56) and (30), respectively.

It is worth noting that this simplified form coincides with the full parametric form in the case of a homogeneous distribution of the isotropic hardening parameter $\bar{\sigma}$ but a heterogeneous distribution of the kinematic hardening parameter $\boldsymbol{\alpha}$; indeed in this case the parametric expressions (38) of $\Sigma_{\text{m}}^{\text{iso}}(\xi)$ and $\Sigma_{\text{eq}}^{\text{iso}}(\xi)$ exactly yield, upon elimination of ξ, the criterion (59), with $\Sigma_1 = \Sigma_2 = \bar{\sigma}$.

4. Assessment of the model

The model will now be assessed by comparing its predictions to the results of some micromechanical finite element simulations of the elementary cell considered in its derivation.

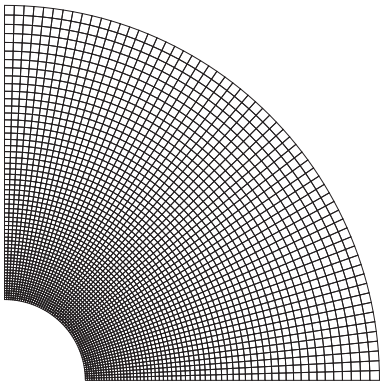

Fig. 2. Spherical mesh used in the finite element calculations ($f = 0.01$).

4.1. Yield surfaces with initial pre-hardening

4.1.1. Description of the simulations

First, in order to study the macroscopic criterion, we consider all internal parameters (geometry and hardening) as fixed. We thus solve the limit-analysis problem for a given, fixed pre-hardening (resulting from some given prestraining), without any geometry update, using the finite element method (FEM).

The calculations are performed with a homemade code using 2D axisymmetric meshes subjected to conditions of homogeneous boundary strain. Fig. 2 shows the mesh used for a void volume fraction $f = 0.01$. Eight-node quadratic elements subintegrated with 2×2 Gauss points are used. The mesh contains 3540 elements and 10,859 nodes (21,718 degrees of freedom). This discretization is adequate for the numerical calculations envisaged, further mesh refinement making no appreciable difference to the results. Axisymmetric loadings are considered: $\Sigma_{11} = \Sigma_{22} \neq 0$, $\Sigma_{33} \neq 0$, and $\Sigma_{ij} = 0$ otherwise. Two Lode angles (denoted θ_L) are considered: $\theta_L = 0$ corresponding to $\Sigma_{33} - \Sigma_{11} > 0$ and $\theta_L = \pi$ corresponding to $\Sigma_{33} - \Sigma_{11} < 0$. The simulations are performed by solving an elastic-plastic evolution problem, the limit-load being considered as reached when the overall stress components no longer evolve (Michel et al., 1999).

4.1.2. Isotropic pre-hardening

We consider two cases with isotropic pre-hardening (and no kinematic pre-hardening: $\boldsymbol{\alpha} = \mathbf{0}$ everywhere in the matrix):

- *Case 1.* Hardening is assumed to be more important near the cavity; the yield stress is supposed to vary linearly with r from the value $\bar{\sigma}(r = a) = 1.5\ \bar{\sigma}_0$ to the value $\bar{\sigma}(r = b) = 0.5\ \bar{\sigma}_0$.
- *Case 2.* Hardening is assumed to be more important near the cell's boundary; the yield stress is supposed to vary linearly with r from the value $\bar{\sigma}(r = a) = 0.5\ \bar{\sigma}_0$ to the value $\bar{\sigma}(r = b) = 1.5\ \bar{\sigma}_0$. Note that this case is probably unrealistic in practice since hardening will likely concentrate near the voids's boundary; it is however interesting to consider it in order to study the robustness of the model.

Fig. 3 compares the yield surfaces associated to the theoretical model of Section 3.2 and its simplified version of Section 3.6 with $N = 10$ phases,[3] Gurson (1977)'s model without pre-hardening and the finite element results, for a porosity $f = 0.01$. Since Gurson (1977)'s model does not account for the different values of the macroscopic yield stresses in the "square" and "cosh" terms of the yield criterion (resulting from the heterogeneous distribution of the local yield stress within the matrix), two values of Gurson's unique "overall yield stress" $\bar{\Sigma}$ (see Appendix A) are envisaged, $\bar{\Sigma} = \Sigma_1$ and $\bar{\Sigma} = \Sigma_2$, these quantities being given by Eq. (56).

Some comments are in order here:

- In the two cases considered, the model developed is in very good agreement with the finite element results for all the triaxialities considered; in particular, the hydrostatic point is perfectly reproduced.
- In both cases, the full and simplified models yield very similar results: the simplified model with an explicit form of the yield criterion thus seems to be a viable alternative to the more complex one.
- The comparison with Gurson (1977)'s model highlights the influence of the heterogeneous distribution of pre-hardening on the strength of the porous material: this model involving a single overall yield limit $\bar{\Sigma}$ can capture either the hydrostatic point or the deviatoric point, depending on the choice made for this overall yield limit, but not both.[4]
- Finally, it is worth noting that the finite element results are slightly sensitive to the Lode angle θ_L (small dissymmetry of the numerical results with respect to the horizontal axis), in contrast to the model developed that does not account for a Lode angle dependency; this is due to Gurson (1977)'s approximation (leading from Eqs. (18) to (19) above) that erases the Lode angle dependency in the macroscopic plastic potential (Cazacu et al., 2013; Leblond and Morin, 2014).

4.1.3. Kinematic pre-hardening

We now consider three cases with kinematic pre-hardening (and no isotropic pre-hardening: $\bar{\sigma} = \bar{\sigma}_0 = Cst.$ everywhere). In all cases the local backstress $\boldsymbol{\alpha}$ is of the form

$$\boldsymbol{\alpha} = \boldsymbol{\alpha}_1(r) + \alpha_2(r)(-2\mathbf{e}_r \otimes \mathbf{e}_r + \mathbf{e}_\theta \otimes \mathbf{e}_\theta + \mathbf{e}_\varphi \otimes \mathbf{e}_\varphi), \tag{61}$$

where the traceless tensor $\boldsymbol{\alpha}_1(r)$ and the scalar $\alpha_2(r)$ depend only on r.

- *Case 1.* Pre-hardening is assumed to affect the sole deviatoric stress; the non-zero components of $\boldsymbol{\alpha}_1$ are: $\alpha_{1(11)} = \alpha_{1(22)} = -\alpha_{1(33)}/2 = -\bar{\sigma}_0/6$ and α_2 is nil.
- *Case 2.* Pre-hardening is assumed to affect the sole hydrostatic stress; α_2 is supposed to vary linearly from the value $\alpha_2(r = a) = -\bar{\sigma}_0/6$ to the value $\alpha_2(r = b) = 0$, and $\boldsymbol{\alpha}_1$ is nil.
- *Case 3.* Pre-hardening is assumed to affect both the hydrostatic and deviatoric stresses; the nonzero components of $\boldsymbol{\alpha}_1$ are $\alpha_{1(11)} = \alpha_{1(22)} = -\alpha_{1(33)}/2 = -\bar{\sigma}_0/4$, and α_2 is supposed to vary linearly from the value $\alpha_2(r = a) = -\bar{\sigma}_0/4$ to the value $\alpha_2(r = b) = 0$.

Fig. 4 compares the yield surfaces associated to the theoretical model developed in Section 3.2 with $N = 30$ phases, Gurson (1977)'s model without pre-hardening (with $\bar{\sigma} = \bar{\sigma}_0$ everywhere in the matrix),[5] and the finite element results, for a porosity $f = 0.01$. (In this case, the simplified model exactly coincides with the more complete one since there is no isotropic pre-hardening, so its predictions need not be shown).

In all three cases considered, the model developed is in very good agreement with the finite element results for all the triaxialities considered; in particular, the model reproduces the "translatory motion" of the yield surface perfectly, in contrast to

[3] In all the simulations, the thickness of the phases has been chosen uniform for simplicity.

[4] The reason why Gurson (1977)'s model fails so utterly to reproduce the numerical results is that the variation of $\bar{\sigma}$ considered here in the matrix is very important; for a more moderate variation the results would have been more acceptable.

[5] Gurson (1977)'s criterion, which does not account for kinematic hardening, is represented with the sole purpose of evidencing the influence of pre-hardening.

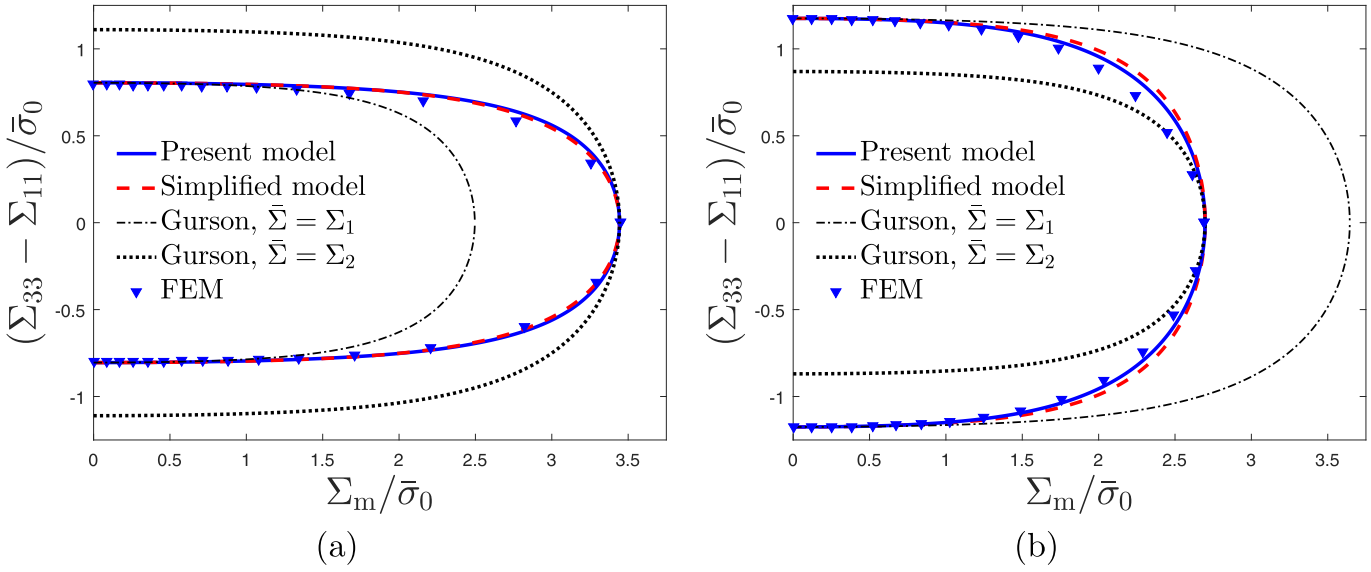

Fig. 3. Yield surfaces for isotropic pre-hardening: theoretical model given by Eq. (38) (Present model), simplified model given by Eq. (60) (Simplified model), Gurson's model (Gurson) and finite element results (FEM). (a) Case 1, (b) Case 2 (see text).

Gurson (1977)'s model without kinematic hardening. As expected from the theoretical form of the criterion, the term $\mathbf{A}_1$ affects only the position of the yield surface in the "deviatoric direction" while the term A_2 affects only its position in the "hydrostatic direction".

4.2. Evolution problems

4.2.1. Description of the simulations

We now wish to compare the model's predictions to the results of micromechanical finite element simulations of *evolution* problems. The hardening is now supposed to evolve locally within the matrix but geometry changes are still disregarded. The motivation for this choice is to comply with the model's hypothesis of spherical voids, in order to assess the sole evolution of the hardening; the modification of the geometry would induce some void shape effects that are disregarded by the model and thus would introduce some discrepancies.

Again, the simulations are performed using 2D axisymmetric meshes subjected to conditions of homogeneous boundary strain (see Fig. 2). The macroscopic stress tensor is constrained to be of the form

$$\mathbf{\Sigma} = C(t)\,\mathbf{\Sigma}^0, \quad \mathbf{\Sigma}^0 = \begin{pmatrix} \Sigma^0_{11} & 0 & 0 \\ 0 & \Sigma^0_{11} & 0 \\ 0 & 0 & \Sigma^0_{33} \end{pmatrix}. \tag{62}$$

In this expression, $C(t)$ is a time-varying scalar and $\mathbf{\Sigma}^0$ is a constant tensor whose components Σ^0_{11} and Σ^0_{33} are given by

$$\Sigma^0_{11} = \cos\beta - \frac{1}{3}\sin\beta, \quad \Sigma^0_{33} = \cos\beta + \frac{2}{3}\sin\beta, \tag{63}$$

where the angle β depends on the stress triaxiality T:

$$\beta = \operatorname{argtan}\left(\frac{1}{T}\right). \tag{64}$$

Only the value $\theta_L = 0$ of the Lode angle is considered, corresponding to $\Sigma_{33} - \Sigma_{11} > 0$. The simulations are performed incrementally, for proportional loading paths - implying a constant stress triaxiality (Michel et al., 1999). Finally the macroscopic strain tensor is denoted $\mathbf{E}$.

We investigate the cases of isotropic hardening and *linear* kinematic hardening. Isotropic hardening is supposed to follow the power-law defined by Eq. (45), and kinematic hardening the law defined by Eq. (49) with $c = Cst.$ and $k = 0$ (no strain recovery).

The values of the material parameters considered are as follows: Young's modulus, $E = 10,000$ GPa, Poisson's ratio, $\nu = 0.25$; isotropic hardening parameters, $\bar{\sigma}_0 = 100$ MPa, $h = 400$ MPa and $m = 0.2$; kinematic hardening slope, $c = 400$ MPa. Note that the value chosen for Young's modulus is extremely high so that elasticity is negligible in the simulations, in agreement with the hypothesis made in the derivation of the model.

The response is investigated for three stress states: (i) pure hydrostatic loading, $T = +\infty$; (ii) high triaxiality, $T = 2.333$; (iii) low triaxiality, $T = 1/3$. We are interested in:

1. *Macroscopic quantities.* We study the evolution of the stress amplitude $C(t)$ versus the "measure of deformation" $\mathbf{E}$: $\mathbf{\Sigma}^0$.
2. *Microscopic quantities - isotropic hardening.* For this type of hardening we study the distribution of the local equivalent von Mises stress σ_{eq} (at the end of the simulation for which $\mathbf{E} : \mathbf{\Sigma}^0 = 0.05$). This variable reduces to the local yield stress $\bar{\sigma}$ in the model which assumes that the matrix is plastic everywhere; but this is not true in the finite element calculations since the material is not necessarily entirely plastic.
3. *Microscopic quantities - kinematic hardening.* For that type of hardening we study the distribution of the local equivalent backstress $\alpha_{\text{eq}} = \sqrt{\frac{3}{2}\boldsymbol{\alpha} : \boldsymbol{\alpha}}$ (at the end of the simulation for which $\mathbf{E} : \mathbf{\Sigma}^0 = 0.05$).

4.2.2. Isotropic hardening

Fig. 5 compares the strain-stress predicted by the model developed with $N = 10$ phases, to that predicted by Gurson (1977)'s classical model including a heuristic modelling of isotropic hardening (see Appendix A), and the results obtained by the finite element method. Note that the predictions of the simplified model are not represented since they are almost indistinguishable from those of the full model for the three cases considered.

The present model's predictions are globally very close to the numerical results in the three cases considered. In the intermediate case ($T = 2.333$) the model slightly overestimate the finite element results. It is worth noting that the very good agreement observed at very low triaxiality ($T = 1/3$) is due in part to the fact that the geometry is not allowed to evolve in the simulations, which ensures that the void remains spherical. Gurson (1977)'s

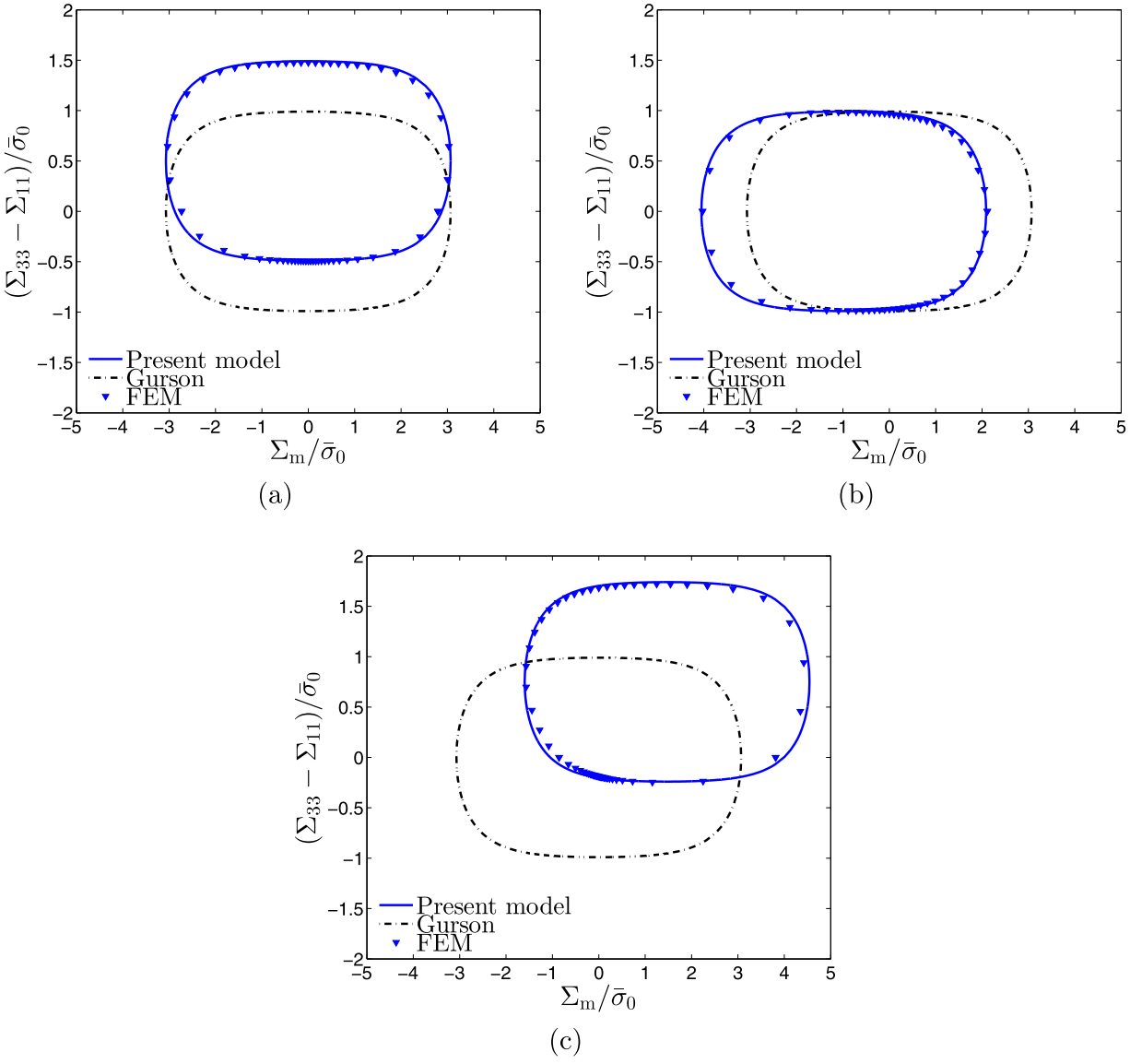

Fig. 4. Yield surfaces for kinematic pre-hardening: theoretical model given by Eq. (38) (Present model), Gurson's model without hardening (Gurson) and finite element results (FEM). (a) Case 1, (b) Case 2, (c) Case 3 (see text).

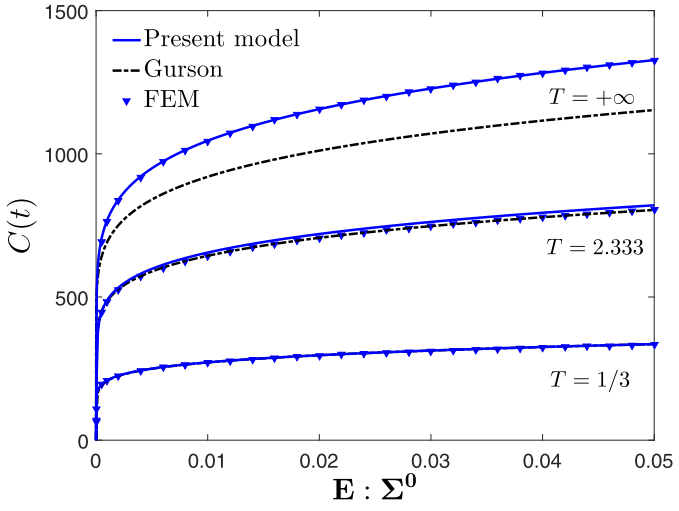

Fig. 5. Stress-strain curve in the case of isotropic hardening: predictions of the present model (Present model), Gurson (1977)'s model with a heuristic modelling of isotropic hardening (Gurson) and finite element results (FEM).

predictions are in good agreement with the numerical results for low and moderate triaxialities but become poor at very high triaxiality. This highlights the detrimental effect of Gurson's hypothesis that the overall yield stresses under purely hydrostatic and purely deviatoric loadings may be related to a single average yield stress of the matrix.

The distribution of the local equivalent von Mises stress is represented in Fig. 6 for the present model and the finite element simulations. The present model globally accurately reproduces the heterogeneous distribution of hardening. In particular, the finite element results reveal that the hypothesis made in the model of an essentially *radial* variation of the yield limit $\bar{\sigma}$ is acceptable. In the case of a pure hydrostatic loading, $T=+\infty$, this approximation becomes exact. In the cases of low or high triaxiality, $T=1/3$ and 2.333, the maps show that the hypothesis of essentially radial dependence is acceptable in a large domain far from the void's boundary, and that the stress level predicted is correct. The hypothesis is no longer verified near the void's boundary, but the angular average of the finite element values is qualitatively well predicted by the model.

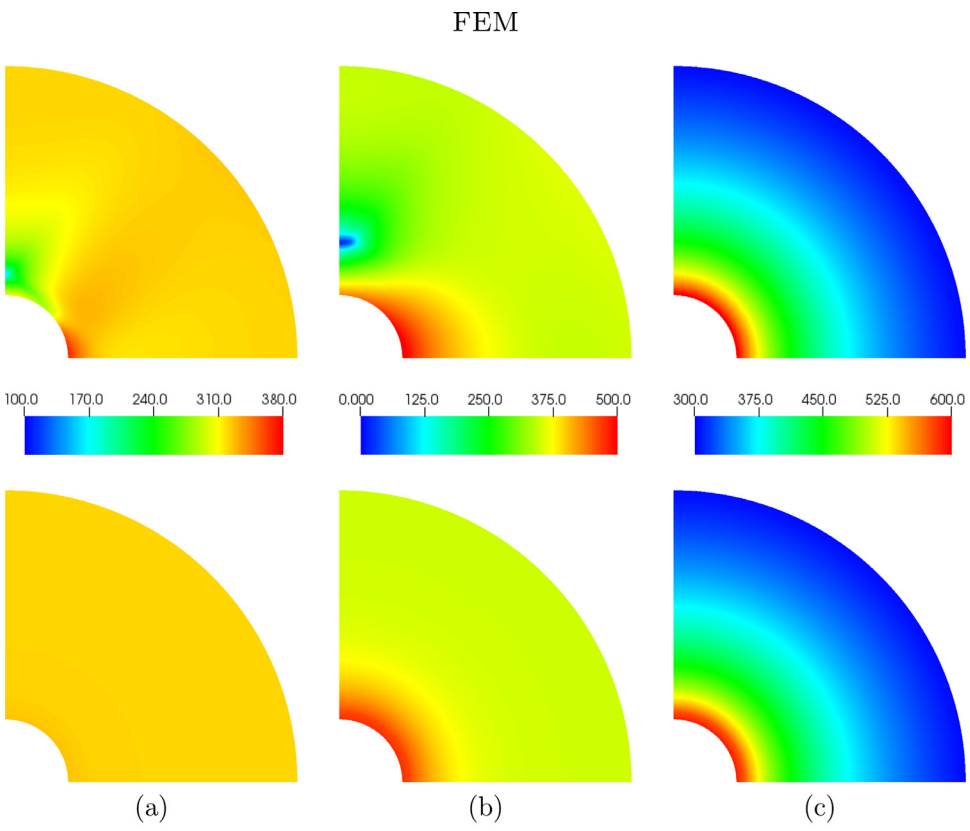

Fig. 6. Distribution of the local equivalent von Mises stress σ_{eq} at $\mathbf{E} : \mathbf{\Sigma}^0 = 0.05$ in the case of isotropic hardening. (a) $T = 1/3$, (b) $T = 2.333$, (c) $T = +\infty$. Top: finite element results, bottom: predictions of the present model.

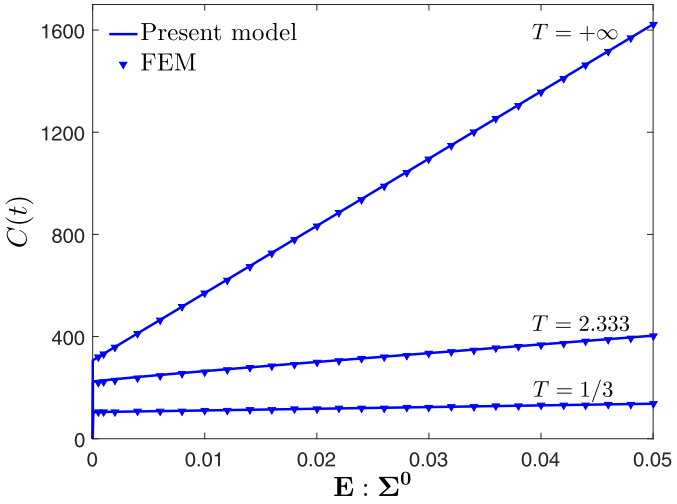

Fig. 7. Stress-strain curve in the case of kinematic hardening: predictions of the present model (Present model) and finite element results (FEM).

4.2.3. Kinematic hardening

Fig. 7 compares the strain-stress curve predicted by the present model with $N = 30$ phases to the results obtained by the finite element method.

In this case, the predictions of the model coincide almost perfectly with the finite element results, emphasizing that the "macroscopic backstresses" $\mathbf{A}_1$ and A_2 are sufficient to capture the effect of the heterogeneous distribution of kinematic hardening. Again it is worth noting that the geometry is not allowed to evolve in the simulations, which ensures that void shape effects are disregarded.

The distribution of the local equivalent backstress α_{eq} predicted by the model is compared in Fig. 8 to the finite element results. The present model globally accurately reproduces the distribution of kinematic hardening. Again, the finite element results also reveal that the hypothesis made in the model about the distribution of $\boldsymbol{\alpha}$ in the phases (Eq. (25)) is acceptable; the comments made above for *isotropic* hardening also apply to *kinematic* hardening. Note, however, that for kinematic hardening, unlike for isotropic hardening, formula (25) predicts some dependence of $\boldsymbol{\alpha}$ upon the spherical angle θ, which is confirmed by the finite element results, see case (b).

4.3. Remarks

It should be noted that the very good results observed for yield surfaces as well as evolution problems have been achieved with a reasonable number of layers ($N = 10$ for isotropic hardening and $N = 30$ for kinematic hardening). These discretizations were found to be sufficient to accurately describe both the macroscopic results and the distributions of microscopic hardening, further refinement making no appreciable difference to the results.

It should be noted too that the model developed, with the number of layers considered, does not require a significantly larger CPU time than Gurson's original model. This is due to the fact that the integration over the layers represents only a small number of operations in the local projection algorithm, representing itself a modest part of the global iterative algorithm. However, the new model requires more memory than Gurson's original model in order to store the internal variables in the layers.

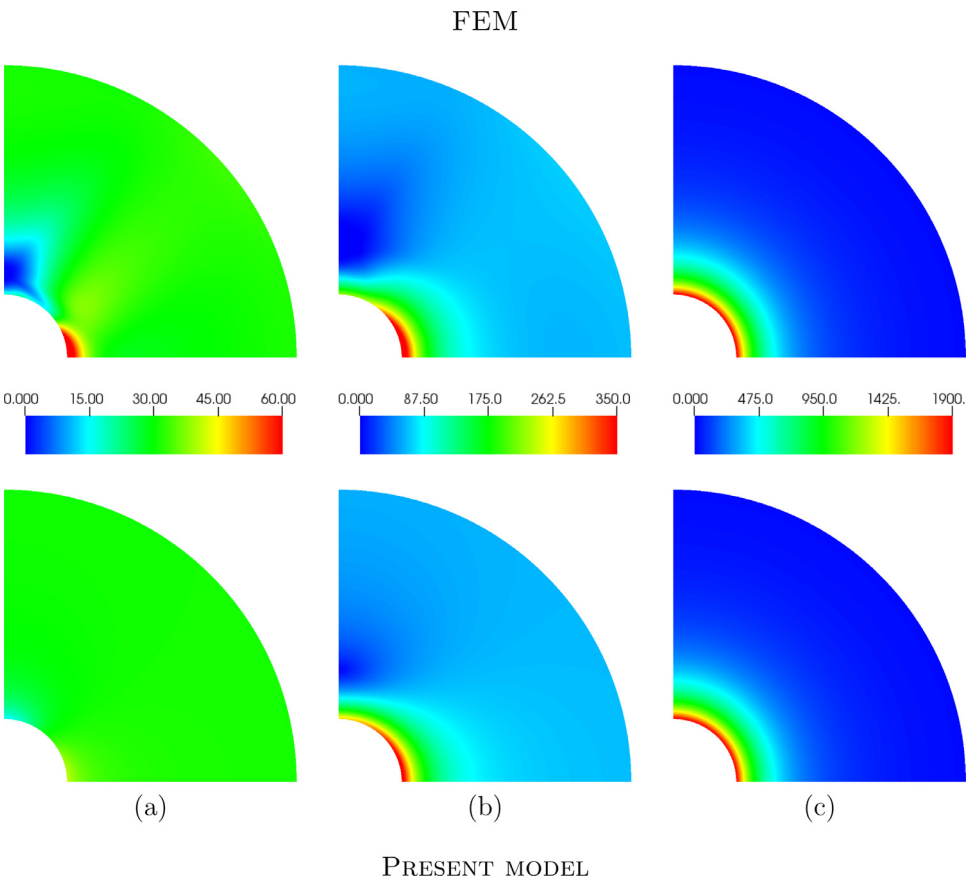

Fig. 8. Distribution of the local equivalent backstress α_{eq} at $\mathbf{E} : \boldsymbol{\Sigma}^0 = 0.05$ in the case of kinematic hardening. (a) $T = 1/3$, (b) $T = 2.333$, (c) $T = +\infty$. Top: finite element results, bottom: predictions of the present model.

5. Conclusion

The aim of this paper was to develop a model for ductile porous materials accounting for both isotropic and kinematic hardening. This model differs (although it is inspired) from that of Gurson (1977) including only isotropic hardening, and also from its extension to kinematic hardening due to Mear and Hutchinson (1985), in that it is no longer based on a purely heuristic and macroscopic approach, but on some detailed analysis of the effect of the heterogeneous distribution of microscopic hardening parameters near the voids.

An approximate yield criterion was derived by performing a "sequential limit-analysis" of a hollow sphere made of a rigid-hardenable matrix. To approximately account for the heterogeneity of hardening, the cell was discretized into a finite number of spherically distributed phases in which the quantities characterizing hardening were considered as homogeneous. The macroscopic yield locus was characterized by an overall criterion expressed in a parametric form, wherein the heterogeneous local hardening parameters were accounted for through macroscopic variables. A simplified version of the model involving an explicit form of the overall criterion was then proposed. This version reduces to Lacroix et al. (2016)'s model in the case of purely isotropic hardening.

The model was assessed numerically using micromechanical finite element simulations. First, overall yield loci were investigated for both isotropic and kinematic pre-hardening: a very good agreement was observed between the numerical results and the predictions of the model. Then these predictions were assessed on evolution problems: they were found to be in very good agreement with the finite element results, with regard to both the overall stress-strain curves and the distributions of isotropic and kinematic hardening parameters.

Future developments of the work will include:

- Numerical micromechanical simulations for cyclic loadings including geometry changes, with some comparisons with the predictions of the present model. Such studies are desirable in order to understand the effect of mixed isotropic/kinematic hardening on the ratcheting of the porosity mentioned in the Introduction.
- Finite element implementation of the model and applications to numerical studies of the ductile rupture of actual test specimens subjected to cyclic loadings.
- Derivation of a model including void shape effects, in order to investigate cyclic ductile rupture under conditions of low stress triaxiality.

Acknowledgments

Fruitful discussions with P. Suquet and D. Kondo are gratefully acknowledged.

Appendix A. Gurson's heuristic approach to isotropic hardening effects in porous ductile materials

Gurson (1977)'s original model was obtained for a rigid-ideal plastic material obeying von Mises's criterion and the associated Prandtl-Reuss flow rule, from an approximate limit-analysis of a hollow sphere made of such a material and subjected to conditions of homogeneous boundary strain rate. The macroscopic yield

criterion obtained read

$$\Phi^G(\boldsymbol{\Sigma}) = \frac{\Sigma_{eq}^2}{\bar{\sigma}_0^2} + 2f\cosh\left(\frac{3}{2}\frac{\Sigma_m}{\bar{\sigma}_0}\right) - 1 - f^2 = 0, \tag{A.1}$$

where $\bar{\sigma}_0$ is the yield stress, uniform in the matrix.

To introduce isotropic hardening effects into the model, instead of pursuing his micromechanical analysis (as was later done by Leblond et al., 1995), Gurson dropped homogenization and limit-analysis and adopted a heuristic approach. This approach consisted in retaining the analytic form (A.1) of the criterion, replacing $\bar{\sigma}_0$ with some "average yield stress" $\bar{\Sigma}$ of the matrix given by:

$$\bar{\Sigma} = g_1(P); \tag{A.2}$$

in this equation $g_1(p)$ denotes the function providing the local yield limit $\bar{\sigma}$ as a function of the local cumulated plastic strain p, like in Section 3.4 above, and P represents some "average equivalent cumulated strain" in the heterogeneous, porous material. The evolution of P was assumed to be governed by the following equation:

$$(1-f)\bar{\Sigma}\dot{P} = \boldsymbol{\Sigma} : \mathbf{D}, \tag{A.3}$$

which expressed the heuristic assumption of equality of the plastic dissipations in the real, heterogeneous porous material and in a fictitious "equivalent" homogeneous material with equivalent cumulated strain P and yield stress $\bar{\Sigma}$.

References

Armstrong, P., Frederick, C., 1966. A mathematical representation of the multiaxial bauschinger effect. Central Electricity Gen-Board and Berkeley Nuclear Laboratories, Research & Development Department Report RD/B/N731, reprinted in Mater. High Temp. 24 (2007), 11–26.

Becker, R., Needleman, A., 1986. Effect of yield surface curvature on necking and failure in porous plastic solids. ASME J. Appl. Mech. 53, 491–499.

Benzerga, A.A., Besson, J., 2001. Plastic potentials for anisotropic porous solids. Eur. J. Mech. A. Solids 20, 397–434.

Benzerga, A.A., Leblond, J.B., 2010. Ductile fracture by void growth to coalescence. Adv. Appl. Mech. 44, 169–305.

Benzerga, A.A., Leblond, J.B., 2014. Effective yield criterion accounting for microvoid coalescence. ASME J. Appl. Mech. 81, 031009.

Benzerga, A.A., Leblond, J.B., Needleman, A., Tvergaard, V., 2016. Ductile failure modeling. Int. J. Fract. 201, 29–80.

Besson, J., Guillemer-Neel, C., 2003. An extension of the Green and Gurson models to kinematic hardening. Mech. Mater. 35, 1–18.

Brocks, W., Steglich, D., 2003. Damage models for cyclic plasticity. Key Eng. Mater. 251–252, 389–398.

Cazacu, O., Revil-Baudard, B., Lebensohn, R.A., Garajeu, M., 2013. On the combined effect of pressure and third invariant on yielding of porous solids with von Mises matrix. ASME J. Appl. Mech. 80, 064501.

Chaboche, J.L., 1991. On some modifications of kinematic hardening to improve the description of ratcheting effects. Int. J. Plast. 7, 661–678.

Devaux, J., Gologanu, M., Leblond, J.B., Perrin, G., 1997. On continued void growth in ductile metals subjected to cyclic loadings. In: Willis, J. (Ed.), Proceedings of the IUTAM Symposium on Nonlinear Analysis of Fracture, Kluwer, Cambridge, GB, pp. 299–310.

Garajeu, M., Michel, J.C., Suquet, P., 2000. A micromechanical approach of damage in viscoplastic materials by evolution in size, shape and distribution of voids. Comput. Methods Appl. Mech. Eng. 183, 223–246.

Gilles, P., Jullien, B., Mottet, G., 1992. Analysis of cyclic effects on ductile tearing strength by a local approach of fracture. In: Advances in Fracture/Damage Models for the Analysis of Engineering Problems, 137. ASME Publication AMD, pp. 269–284.

Gologanu, M., Leblond, J.B., Devaux, J., 1993. Approximate models for ductile metals containing non-spherical voids-case of axisymmetric prolate ellipsoidal cavities. J. Mech. Phys. Solids 41, 1723–1754.

Gologanu, M., Leblond, J.B., Devaux, J., 1994. Approximate models for ductile metals containing nonspherical voids—case of axisymmetric oblate ellipsoidal cavities. ASME J. Eng. Mater. Technol. 116, 290–297.

Gologanu, M., Leblond, J.B., Perrin, G., Devaux, J., 1997. Recent extensions of Gurson's model for porous ductile metals. In: Suquet, P. (Ed.), Continuum Micromechanics, CISM Courses and Lectures. Springer-Verlag, 377, pp. 61–130.

Gurson, A.L., 1977. Continuum theory of ductile rupture by void nucleation and growth: part I—yield criteria and flow rules for porous ductile media. ASME J. Eng. Mater. Technol. 99, 2–15.

Herve, E., Zaoui, A., 1993. N-layered inclusion-based micromechanical modelling. Int. J. Eng. Sci. 31, 1–10.

Keralavarma, S., Benzerga, A., 2010. A constitutive model for plastically anisotropic solids with non-spherical voids. J. Mech. Phys. Solids 58, 874–901.

Kobayashi, H., Kusumoto, T., Nakazawa, H., 1992. The cyclic J-R curve and upper-limit characteristic of fatigue-crack growth in 2-1/2 Cr-Mo steel. Int. J. Press. Vessels Pip. 52, 337–356.

Lacroix, R., Leblond, J.B., Perrin, G., 2016. Numerical study and theoretical modelling of void growth in porous ductile materials subjected to cyclic loadings. Eur. J. Mech. A. Solids 55, 100–109.

Leblond, J.B., Morin, L., 2014. Gurson's criterion and its derivation revisited. ASME J. Appl. Mech. 81, 051012.

Leblond, J.B., Perrin, G., Devaux, J., 1995. An improved Gurson-type model for hardenable ductile metals. Eur. J. Mech. A. Solids 14, 499–527.

Leu, S.Y., 2007. Analytical and numerical investigation of strain-hardening viscoplastic thick-walled cylinders under internal pressure by using sequential limit analysis. Comput. Methods Appl. Mech. Eng. 196, 2713–2722.

Madou, K., Leblond, J.B., 2012. A gurson-type criterion for porous ductile solids containing arbitrary ellipsoidal voids—i: limit-analysis of some representative cell. J. Mech. Phys. Solids 60, 1020–1036.

Madou, K., Leblond, J.B., 2012. A gurson-type criterion for porous ductile solids containing arbitrary ellipsoidal voids—II: determination of yield criterion parameters. J. Mech. Phys. Solids 60, 1037–1058.

Madou, K., Leblond, J.B., 2013. Numerical studies of porous ductile materials containing arbitrary ellipsoidal voids—i: yield surfaces of representative cells. Eur. J. Mech. A. Solids 42, 480–489.

Madou, K., Leblond, J.B., Morin, L., 2013. Numerical studies of porous ductile materials containing arbitrary ellipsoidal voids—II: evolution of the length and orientation of the void axes. Eur. J. Mech. A. Solids 42, 490–507.

Mbiakop, A., Constantinescu, A., Danas, K., 2015. On void shape effects of periodic elasto-plastic materials subjected to cyclic loading. Eur. J. Mech. A. Solids 49, 481–499.

Mear, M.E., Hutchinson, J.W., 1985. Influence of yield surface curvature on flow localization in dilatant plasticity. Mech. Mater. 4, 395–407.

Michel, J.C., Moulinec, H., Suquet, P., 1999. Effective properties of composite materials with periodic microstructure: a computational approach. Comput. Methods Appl. Mech. Eng. 172, 109–143.

Monchiet, V., Cazacu, O., Charkaluk, E., Kondo, D., 2008. Macroscopic yield criteria for plastic anisotropic materials containing spheroidal voids. Int. J. Plast. 24, 1158–1189.

Morin, L., Kondo, D., Leblond, J.B., 2015. Numerical assessment, implementation and application of an extended Gurson model accounting for void size effects. Eur. J. Mech. A. Solids 51, 183–192.

Morin, L., Leblond, J.B., Benzerga, A.A., 2015. Coalescence of voids by internal necking: theoretical estimates and numerical results. J. Mech. Phys. Solids 75, 140–158.

Morin, L., Leblond, J.B., Kondo, D., 2015. A Gurson-type criterion for plastically anisotropic solids containing arbitrary ellipsoidal voids. Int. J. Solids Struct. 77, 86–101.

Pineau, A., Benzerga, A.A., Pardoen, T., 2016. Failure of metals i: brittle and ductile fracture. Acta Mater. 107, 424–483.

Rabold, F., Kuna, M., 2005. Cell model simulation of void growth in nodular cast iron under cyclic loading. Comput. Mater. Sci 32, 489–497.

Schmidt, R.A., Wilkowski, G.M., Mayfield, M.E., 1991. The International Piping Integrity Research Group (IPIRG) program. An overview. In: 11th International Conference on Structural Mechanics in Reactor Technology (SMIRT 11), Tokyo, Japan, Paper G/23/1.

Steglich, D., Pirondi, A., Bonora, N., Brocks, W., 2005. Micromechanical modelling of cyclic plasticity incorporating damage. Int. J. Solids Struct. 42, 337–351.

Tekoglu, C., Leblond, J.B., Pardoen, T., 2012. A criterion for the onset of void coalescence under combined tension and shear. J. Mech. Phys. Solids 60, 1363–1381.

Thomason, P.F., 1985. Three-dimensional models for the plastic limit-loads at incipient failure of the intervoid matrix in ductile porous solids. Acta Metall. 33, 1079–1085.

Yang, W.H., 1993. Large deformation of structures by sequential limit analysis. Int. J. Solids Struct. 30, 1001–1013.